termis.

Tissue Engineering
& Regenerative Medicine
International Society

ORIGINAL ARTICLE

Bone Tissue Engineering with Multilayered Scaffolds— Part I: An Approach for Vascularizing Engineered Constructs *In Vivo*

Binulal Nelson Sathy, PhD,[1] Ullas Mony, PhD,[1] Deepthy Menon, PhD,[1] V.K. Baskaran, MD,[2] Antonios G. Mikos, PhD,[3] and Shantikumar Nair, PhD[1]

Obtaining functional capillaries through the bulk has been identified as a major challenge in tissue engineering, particularly for critical-sized defects. In the present study, a multilayered scaffold system was developed for bone tissue regeneration, designed for through-the-thickness vascularization of the construct. The basic principle of this approach was to alternately layer mesenchymal stem cell-seeded nanofibers (osteogenic layer) with microfibers or porous ceramics (osteoconductive layer), with an intercalating angiogenic zone between the two and with each individual layer in the microscale dimension (100–400 µm). Such a design can create a scaffold system potentially capable of spatially distributed vascularization in the overall bulk tissue. In the cellular approach, the angiogenic zone consisted of collagen/fibronectin gel with endothelial cells and pericytes, while in the acellular approach, cells were omitted from the zone without altering the gel composition. The cells incorporated into the construct were analyzed for viability, distribution, and organization of cells on the layers and vessel development *in vitro*. Furthermore, the layered constructs were implanted in the subcutaneous space of nude mice and the processes of vascularization and bone tissue regeneration were followed by histological and energy-dispersive X-ray spectroscopy (EDS) analysis. The results indicated that the microenvironment in the angiogenic zone, microscale size of the layers, and the continuously channeled architecture at the interface were adequate for infiltrating host vessels through the bulk and vascularizing the construct. Through-the-thickness vascularization and mineralization were accomplished in the construct, suggesting that a suitably bioengineered layered construct may be a useful design for regeneration of large bone defects.

Introduction

THROUGH-THE-THICKNESS vascularization of engineered tissue is one of the critical challenges in tissue engineering.[1–4] Several approaches are being investigated to achieve functional vascularization in engineered tissues similar to that seen *in vivo*.[4–8] However, less than optimal scaffold architecture remains as one of the crucial factors, which affect the depth, rate of vascular ingrowth, and spatial distribution of vessels in the engineered construct.[9–12] Both angiogenesis, where the development of new vessels occurs from pre-existing blood vessels, and vasculogenesis, where blood vessels are formed through the *de novo* differentiation of stem cells into endothelial cells and/or their progenitors, have been studied by researchers to overcome the problem

of inadequate vascularization of tissue-engineered constructs.[13] For functional vascularization of the construct, the role of material-driven properties such as compatibility, functionality, mechanical property, and degradation along with scaffold design parameters such as structure, porosity, pore size, and interconnectivity are important.[2,5,14–17] The present work addresses this bioengineering problem at the interface of scaffold engineering and the biology of vascularization by offering a new and innovative solution.

The basis for this solution is that in natural tissues, vessels are distributed every 100–200 µm in the tissue, which is the diffusion limit of oxygen.[18] While incorporation of optimal porosity, pore size, and pore interconnectivity to the scaffold has shown some success in obtaining functional vessels into the core of the construct,[12,19,20] to date, any bone scaffold

[1]Amrita Centre for Nanosciences and Molecular Medicine, Amrita Institute of Medical Sciences and Research Centre, Amrita Vishwa Vidyapeetham University, Kochi, India.
[2]Department of Orthopaedics, Amrita Institute of Medical Sciences and Research Centre, Amrita Vishwa Vidyapeetham University, Kochi, India.
[3]Department of Bioengineering, Rice University, Houston, Texas.

construct of macroscopic dimension regardless of pore size and structure has generally failed to get vascularized with functional vessels having spatial distribution similar to that seen *in vivo*. The bioengineered construct developed and investigated in this study is the combination of alternating 100–400 μm thick layers of osteogenic and osteoconductive zones with angiogenic/vasculogenic zones located at their interfaces. This is a scalable construct that can be readily developed into macroscopic implants. Such an architectural construct is hypothesized as a solution for the bottleneck of scaffold vascularization in terms of spatial distribution of vessels so as to ensure availability of oxygen and nutrient supply and effective metabolic waste removal throughout the construct after *in vivo* implantation.

Electrospun polymeric fibers in nanoscale dimensions and calcium phosphate ceramics have been extensively used as scaffolding platforms in various tissue regeneration approaches.[21,22] Polymeric nanofibers produced by electrospinning are attractive due to their similarity to the structural dimensions of native extracellular matrix (ECM).[23] Electrospun microfibers are also used widely especially due to their relatively large interconnected porosity.[24] Products based on calcium phosphate ceramics as interconnected macroporous blocks or granules, alone or in combination with other polymers or bioactive factors, are currently in clinical use. The major criticism against the use of electrospun polymeric nanofibers in tissue engineering is their small pore size and thereby the fish-net effect, which restricts the infiltration of cells and vasculature.[25,26] However, wafers of functional cells in microscale thickness (50–100 μm, the stretchable length of a cell) can be successfully developed using biodegradable nanofibrous wafer discs and appropriate cell seeding strategy. Similarly, porous microfibrous and ceramic discs can be developed in microscale thickness by appropriate methods and can be used as suitable platform for tissue/vessel ingrowth after appropriate bioengineering.

Therefore, this study was focused on developing a design philosophy for multilayered constructs aiming for through-the-thickness vascularization in every 100–200 μm and bone formation. The structural units of the layered construct, such as osteogenic, angiogenic, and osteoconductive layers, in microscale thickness were separately bioengineered and assembled as a single construct. The effect of the continuous channels with vessel-permeable gel at the osteogenic–osteoconductive interfaces, the structural dimensions and architecture of the construct, and the role of cells were investigated for the through-the-thickness vessel formation in an *in vivo* ectopic model. In the companion article,[27] the best performing construct is investigated in a more realistic bone defect model wherein combined vascularization and bone formation can be studied.

Materials and Methods

Bioconstruct design

Osteoconductive layer. Two separate osteoconductive layers were prepared: one with macroporous hydroxyapatite (HAp) discs and the other with microfibrous electrospun polycaprolactone (PCL) discs containing gelatin nanoparticles (nG). One or the other of these two layer choices was used in the final construct, but not both of these together in the same construct.

The thickness of this layer is ∼400 μm, but with the two distinct material choices. HAp is clearly a well-established osteoconductive material[28]; however, PCL has also been extensively investigated for bone formation.[29] A microfibrous layer provides larger and more interconnected porosity for vascular ingrowth, and our own previous study[30] showed that the presence of gelatin nanoparticles (nG) makes electrospun PCL fibers more favorable for mesenchymal stem cells (MSCs). Both these options have been investigated in this study. HAp particles were prepared as previously reported.[31] HAp discs were prepared by the dry compaction method and naphthalene was used as porogen to create microporosity. For the preparation, HAp particles were mixed with naphthalene (Nice Chemicals, Kochi, India) at 1:1 ratio in a custom-designed dye having a bore size of 8 mm diameter (Supplementary Fig. 1; Supplementary Data are available online at www.liebertpub.com/tea) and compressed using a manual hydraulic press (15-Ton Manual Laboratory Press; Kimaya Engineers, Thane, India) to make 8-mm diameter ceramic discs having ∼400 μm thickness. Prepared discs were sintered in a muffle furnace (High Heat, Kochi, India) at 1000°C for 1 h. Sintered ceramic discs were characterized using scanning electron microscopy (SEM) (JSM-6490LA; Jeol, Akishima-shi, Japan) and X-ray diffractometry (XRD) (X'pert PRO; PANalytical, Almelo, The Netherlands). The morphology and pore distribution were evaluated using a SEM and Fourier transform infrared spectroscopy (FTIR) (Spectrum RX1; Perkin-Elmer, Waltham, MA). These porous discs were used as osteoconductive ceramic zones in the layered construct.

For the other layer option, nG were prepared as previously reported[30] and microfibers containing nG were electrospun from 30 wt% PCL_nG solution containing 15 wt% gelatin nanoparticles using a flow rate of 1 mL/h, voltage 10 KV, and tip target distance of 10 cm. Prepared electrospun sheets of about 400 μm thickness were made as 8-mm diameter discs using a skin biopsy punch.

Osteogenic layer: development of PCL nanofibers containing gelatin nanoparticles. Our previous studies have shown that electrospun nanofibrous PCL, by virtue of its nanoscale dimensions, is cell compatible, favoring rapid MSC proliferation and osteogenic differentiation.[30] We have selected such a layer dispersed with gelatin nanoparticles as the osteogenic construct. Gelatin nanoparticles containing PCL_nG composite fibers were prepared as we previously reported.[30] Briefly, 16 wt% PCL solution containing 15 wt% of gelatin nanoparticles was electrospun using a flow rate of 1 mL/h, voltage 10 KV, and tip target distance of 10 cm. Nanofibrous discs of about 100 μm thickness were made using an 8 mm diameter skin biopsy punch from the electrospun sheet.

Nanofibrous osteogenic zones were engineered by dual seeding of human MSCs (hMSCs) on electrospun PCL_nG scaffolds. Scaffolds having 8 mm diameter (100 μm thickness), obtained from using biopsy punches, were placed in a custom-designed scaffold holder (Supplementary Fig. 2). Scaffold holders along with scaffolds were kept in 12-well plates. hMSCs (passages 2–3) differentiated to osteogenic lineage by growing them in osteogenic media[32] for 4 days were seeded on the scaffolds (1×10^5 cells/side). After 4 h, scaffolds were flipped along with the scaffold holders and

the seeding was repeated to make sure cells were on both surfaces of the nanofibrous wafer. To visualize cells on both sides of the nanofibers, nanofibrous discs were cryosectioned (CM1510S3; Leica Biosystems GmbH, Nussloch, Germany) and stained with DAPI (Sigma, St. Louis, MO) and imaged using a fluorescent microscope (BX-51; Olympus Corporation, Shinjuku, Japan) attached with a cooled color CCD camera (Model DP71; Olympus Corporation). The nanofibrous scaffolds seeded with osteogenic differentiation-induced hMSCs are hereafter mentioned as osteogenic zones.

Angiogenic zone: collagen/fibronectin gel with (G+C+) or without (G+C−) human umbilical vein endothelial cells and pericytes. Collagen/fibronectin gel containing human umbilical vein endothelial cells (HUVECs) and pericytes was prepared as previously reported.[33] Collagen solution (Advanced BioMatrix, Carlsbad, CA) containing 90 µg/mL fibronectin (Advanced BioMatrix) and 25 mM HEPES (Sigma) was prepared at 4°C and was mixed with 10× RPMI in a 9:1 ratio. pH of the solution was adjusted by using 1 N NaOH (Sigma). To this solution, 1×10^6 HUVECs and 2.5×10^5 hMSCs predifferentiated into pericytes were added per mL. This suspension was pipetted above the osteoconductive discs and warmed to 37°C for 30 min to allow polymerization of collagen. Soon after formation of the gel, it was covered by carefully adding prewarmed EGM-2 media (Lonza, Basel, Switzerland) and kept in the CO_2 incubator. Acellular angiogenic zones for *in vivo* evaluation were developed by omitting HUVECs and pericytes.

Development and characterization of macroscopic three-dimensional layered constructs. The basic structural unit of the scaffold was a three-layer construct with an angiogenic zone sandwiched between one osteogenic zone and an osteoconductive zone. Accordingly, there were two basic structural units: one with the osteoconductive zone using microfibrous PCL and the other with this layer made from microporous HAp. Extension of either of these structural units in the thickness direction could provide a macroscopic construct for implantation. Such extended three-dimensional (3D) layered constructs were engineered by aseptically layering all zones repetitively within a specially designed holder.

The morphology and structural organization of the layered constructs were evaluated using SEM after sectioning the layered constructs using cryotome (CM1510S3; Leica Biosystems GmbH). The compressive strength of the layered constructs was evaluated using a mechanical tester (Model 4505; Instron, Norwood, MA) with 10 kN load cell. The crosshead speed was set at 0.4 mm/min, and the load was applied until the scaffold was crushed. Averages of five measurements were used to compare the compressive strength of the constructs.

Cells, characterization, and in vitro *and* in vivo
implantation studies

Isolation and characterization of endothelial cells from the umbilical cord. Endothelial cells were isolated from human umbilical cord by slightly modifying the previously reported protocol.[34] The umbilical cord was collected from the Gy-

naecology Department of Amrita Institute of Medical Sciences with the approval of the respective institutional review board and with appropriate informed patient consent. The outer surface of the collected cord (approximate length 20 cm) was cleaned with phosphate-buffered saline (PBS) (Sigma). At one end of the umbilical vein in the cord, a feeding needle was carefully inserted without damaging the surrounding tissue and it was properly held in place using a clamping scissor. The needle was connected with a 20-mL syringe filled with 20 mL PBS containing 2 mM EDTA (Sigma). The vein was rinsed thoroughly using PBS. After proper rinsing, the syringe was replaced with a second syringe filled with 5 mL of prewarmed 0.25% trypsin-EDTA (Sigma). The other end of the vein was closed by connecting to a needle with an end cap and clamping it with a clamping scissor. Into the vein, 5 mL of the prewarmed trypsin-EDTA solution was injected. Then, the cord was suspended in U shape in a beaker containing 500 mL of prewarmed sterile distilled water and incubated at 37°C for 15–20 min. After incubation, the cord was placed on soft sterile cotton and massaged aseptically in the hood for 5 min with two fingers. Another syringe with 8 mL of PBS containing 2 mM EDTA was connected to the feeding needle. The needle end cap from the other end of the cord was removed and the cord was flushed with PBS containing 2 mM EDTA to a 50-mL falcon tube containing 2 mL fetal bovine serum (FBS). The elute was centrifuged at 200 g and the supernatant was carefully aspirated. The pellet was suspended in 15 mL endothelial growth media (EGM-2 BulletKit; Lonza) and cells were directly plated in gelatin-coated T75 flasks. Unattached cells were removed after 6 h and the attached cells were passaged at 80% confluency. HUVECs at passages 2–3 were characterized using immunocytochemistry and low-density lipoprotein (LDL) uptake.

For immunocytochemistry, HUVECs were seeded onto the gelatin-coated coverslips and incubated in EGM-2 growth media. After 24 h, cells were fixed with 4% paraformaldehyde and were blocked with 1% bovine serum albumin (BSA) in PBS for 30 min to minimize unspecific binding of the antibodies. Blocked cells were incubated with the diluted (1:1000) FITC-conjugated mouse anti-human CD-31 (Sigma-Aldrich, St. Louis, MO) antibody in 1% BSA in PBS in a humidified chamber for 1 h at room temperature. After incubation, cells were washed thrice with PBS and were mounted using Vectashield (Vector Labs, Burlingame, CA). Mounted coverslips were sealed with sealants to prevent drying and movement under the microscope and evaluated using confocal microscopy.

Acetylated low-density lipoprotein (AcLDL) uptake by HUVECs was evaluated by visualizing the uptake using DiI-conjugated AcLDL. For the assay, HUVECs were seeded on gelatin-coated coverslips and incubated with 10 µg/mL DiI-Ac-LDL (Invitrogen, Carlsbad, CA) at 37°C in serum-free EGM-2 media. After 4 h, media were removed and the cells were washed twice with PBS. They were fixed with 4% paraformaldehyde, mounted as mentioned above, and visualized using the confocal microscope (TCS SP5 II; Leica Microsystems, Mannheim, Germany).

Isolation and culturing of hMSCs. hMSCs were isolated and characterized as we previously reported.[32] Passage 2–3 cells were used for all experiments.

Predifferentiation of hMSCs to pericytes and characterization. hMSCs were predifferentiated to pericytes using transforming growth factor-beta (TGF-β) treatment as previously reported.[35] Passage 2 MSCs were seeded in T75 flasks in α-MEM containing 20% FBS (Stem Cell Technologies, Vancouver, Canada) and 50 U mL^{-1} penicillin–streptomycin (Invitrogen) containing 1 ng/mL TGF-β for 5 days. After 5 days, cells were characterized based on the smooth muscle cell-specific marker expression. For characterization, cells were fixed with 4% paraformaldehyde in PBS and permeabilized with 0.1% Triton X-100 in PBS for 5 min. Permeabilized cells were blocked with 1% BSA in PBS for 15 min and incubated with primary antibodies against smooth muscle α-actin (Sigma) and calponin (Sigma) (1:1000) for 1 h at room temperature. After 1 h, unbound antibodies were removed by washing in PBS twice and were incubated with fluorochrome-labeled secondary antibodies for 1 h (anti-mouse IgG-Alexa fluor 488 and anti-mouse IgG-Texas red, 1:500) (Invitrogen). After incubation, unbound secondary antibodies were washed away using PBS and samples were mounted and visualized using the confocal microscope.

In vitro evaluation of the microvascular network formation in the angiogenic zone. Localization of endothelial cells and pericytes in the angiogenic zone and the *in vitro* vascular network formation were evaluated using prelabeled HUVECs and pericytes and by calcein staining, respectively. Both HUVECs and pericytes were prelabeled using lipophilic dyes, PKH 26 and PKH67 (Sigma), as per the manufacturer's protocol. HUVECs were labeled with red dye (PKH 26) and pericytes were labeled with green dye (PKH67). For labeling, 1 mL cell suspension containing 2×10^7 HUVECs or pericytes was taken in a 15-mL tube and washed with serum-free media. Then, cells were centrifuged at 400 g to get a loose pellet. The supernatant was carefully aspirated completely without disturbing the pellet. One milliliter of diluent C is added to the pellet and it was resuspended with gentle trituration. Immediately before staining, a 2× dye solution was prepared (green dye for pericytes and red dye for HUVECs) in diluent C by adding the appropriate amount of the dye to the diluent solution. One milliliter of 2× dye solution was rapidly added to 1 mL of 2× cell suspension and mixed by gentle trituration. The cell–dye suspension was incubated for 5 min, after which 2 mL of serum was added to the solution to stop the reaction. The cells were centrifuged at 400 g for 10 min at 20–25°C and the supernatant was carefully removed. The cells were resuspended in 10 mL of complete media and transferred to a fresh 15-mL tube and centrifuged at 400 g for 5 min at 20–25°C. This procedure was repeated thrice. After the final wash, cells were suspended in 10 mL of complete media and the required number of cells for angiogenic zone preparation was added to the collagen/fibronectin gel solution in both the microfibrous polymeric platform and microporous ceramic platform. Prepared angiogenic zones were incubated in endothelial growth media for 1 day and were evaluated for vascular network formation using live cell imaging facility in the confocal microscope.

For calcein staining, angiogenic zones with unlabeled cells were incubated in complete endothelial media (EGM-2) for 48 h. At 5 days, cells in the angiogenic zones were stained with calcein (Invitrogen). Briefly, 2 μM calcein solution was prepared in sterile PBS from the 4 mM stock. The angiogenic zones were taken out from the scaffold holders and placed in confocal microscopic dishes (ibidi GmbH, Planegg, Germany) containing 200 μl of prepared calcein solution. Angiogenic zones were incubated in the calcein solution for 30–45 min and were imaged in the live cell imaging facility of the confocal microscope.

Subcutaneous implantation and *in vivo* evaluation of the layered constructs. The ectopic animal model used in the present study has been reported elsewhere.[36] All animal studies were carried out in accordance with the Institutional Animal Ethics Committee (IAEC) and Committee for the Purpose of Control and Supervision of Experiments on Animals (CPCSEA) (India). Layered constructs were subcutaneously implanted on the flanks of athymic mice (Nude-HSD-Fox N1).

Viability of cells on the osteogenic zone after implantation was evaluated 48 h after implantation. Under anesthesia, constructs were surgically removed from representative animals at 48 h after implantation. Live–dead and Alamar blue assay were performed on osteogenic zones to evaluate the survival of implanted cells *in vivo*. At 28 days, animals were sacrificed using overdose of anesthetics and the constructs were surgically removed and stored in 10% neutral buffered formalin solution. Constructs were processed and embedded in methyl methacrylate (Sigma). Thick sections (70–100 μm) were made from the poly(methyl methacrylate) blocks through the middle of the constructs using a linear precision saw microtome (ISOMET 5000; Buehler GmbH, Dusseldorf, Germany). Sections containing the center points were stained with hematoxylin–eosin (HE; Sigma) and imaged. Vascularization and tissue regeneration were analyzed and quantified using image analysis software, ImageJ (National Institute of Health). For the analysis of mineralization in the osteogenic zones, the nanofibrous layers of representative samples were surgically removed from the layered constructs and energy-dispersive X-ray spectroscopy (EDS) analysis was performed.
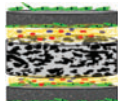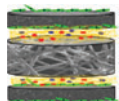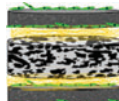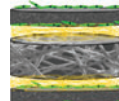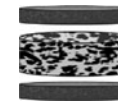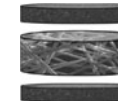
Experimental groups

Constructs were categorized into three major groups. Group-1 contained layered constructs where angiogenic zones with cells were used with bioengineered osteogenic and osteoconductive zones. Group-2 contained layered constructs where acellular angiogenic zones were used with bioengineered osteogenic and osteoconductive zones. Group-3 contained layered constructs with nanofibers and osteoconductive zones without any angiogenic zone. Each group was subdivided into two based on the osteoconductive platforms as shown in Table 1.

Statistical analysis

Quantitative results are represented as mean ± standard deviation. Student's *t*-test was performed to determine statistical significance on *in vitro* results. Multifactor analysis of variance, followed by a Tukey–Kramer multiple comparisons test, was performed on *in vivo* results using

TABLE 1. EXPERIMENTAL GROUPS

Representation	Group-1		Group-2		Group-3	
	A $N^{C+}C^{G+C+}$	B $N^{C+}M^{G+C+}$	A $N^{C+}C^{G+C-}$	B $N^{C+}M^{G+C-}$	A $N^{C-}C^{G-C-}$	B $N^{C-}M^{G-C-}$
Nanofiber (N)	✓	✓	✓	✓	✓	✓
MSCs (C^+)	✓	✓	✓	✓	—	—
Microfiber (M)	—	✓	—	✓	—	✓
Ceramic (C)	✓	—	✓	—	✓	—
Collagen/fibronectin gel (G^+)	✓	✓	✓	✓	—	—
HUVECs and pericytes (C^+)	✓	✓	—	—	—	—
Multilayered scaffolds						

HUVECs, human umbilical vein endothelial cells; MSCs, mesenchymal stem cells.
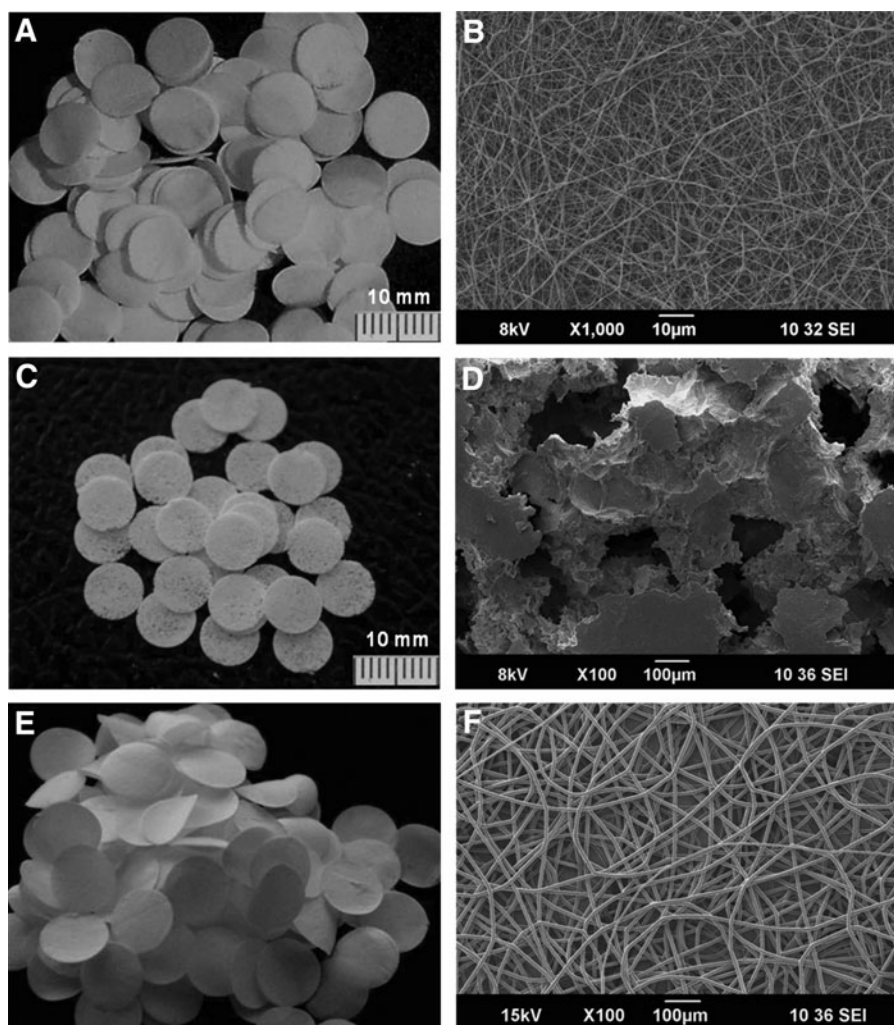

FIG. 1. Scaffolds developed for osteogenic and angiogenic zones. **(A, C, E)** Representative photographs of the nanofibrous, ceramic, and microfibrous discs. Corresponding scanning electron microscopy (SEM) images showing the structural dimensions of the scaffolds and its pore size are shown in **B, D,** and **F,** respectively.
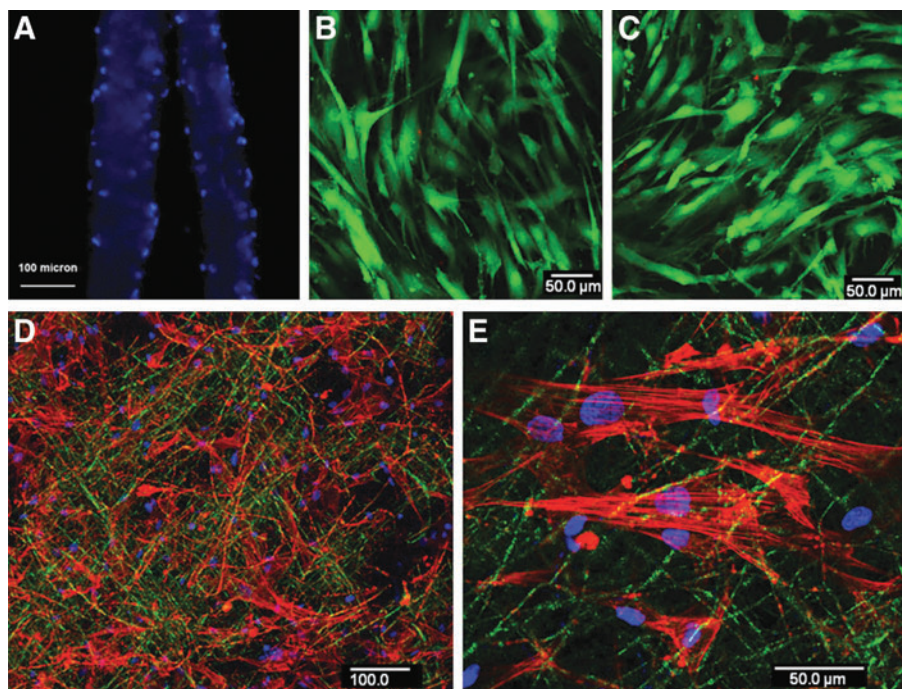
FIG. 2. Mesenchymal stem cells (MSCs) on the osteogenic zone. **(A)** The cryosection of the MSC-seeded (dual seeding) nanofibrous wafers (two wafers) after staining with DAPI confirmed the presence of cells on both sides. **(B, C)** Confocal microscopic images of the *top* and *bottom* sides of the dual-seeded nanofibrous wafer at 24 h after live–dead staining and *green* staining indicate live cells. **(D)** The representative confocal microscopic image of the nanofibrous osteogenic zone stained for F-actin counterstained by DAPI at 24 h after seeding with human MSCs (hMSCs). **(E)** The higher magnification image showing the actin filament organization of MSCs on the osteogenic zone.

GraphPad Prism analysis software. In both the cases, $p < 0.05$ was considered to be statistically significant.

Results

Nanofibrous, microfibrous, and ceramic scaffolds

Developed osteogenic, osteoconductive, and angiogenic scaffolding platforms had a diameter of 8 mm (Figs. 1A–D). The thickness of the nanofibrous layer was ≤100 µm and microfibrous and ceramic layer was ≤400 µm (Figs. 2A and 6B). The ceramic discs showed characteristic IR spectra and characteristic XRD peaks of HAp (Supplementary Fig. 3). The pore size in the nanofibrous discs was smaller than the size of a cell, whereas microfibrous as well as ceramic scaffolds showed macropores (Figs. 1B, D, F).

Osteogenic layer. Osteogenic zones developed on the electrospun nanofibrous discs by dual seeding (on both sides of the layer) of MSCs showed cells on both sides of the nanofibrous wafer as shown in Figure 2A. The total thickness of the osteogenic zones was <100 µm. Seeded cells on both sides of the nanofibrous wafer were viable at 1 week of osteogenic induction (Figs. 2B, C) and showed well-organized actin filaments.

Angiogenic zone. Isolated HUVECs showed typical cobblestone morphology of endothelial cells as previously reported[37] (Fig. 3A). They uniformly stained positive for endothelial cell marker, CD31, and showed positive results for acetylated LDL uptake as shown in Figures 3B and C, respectively. MSCs treated with TGF-β for 5 days showed
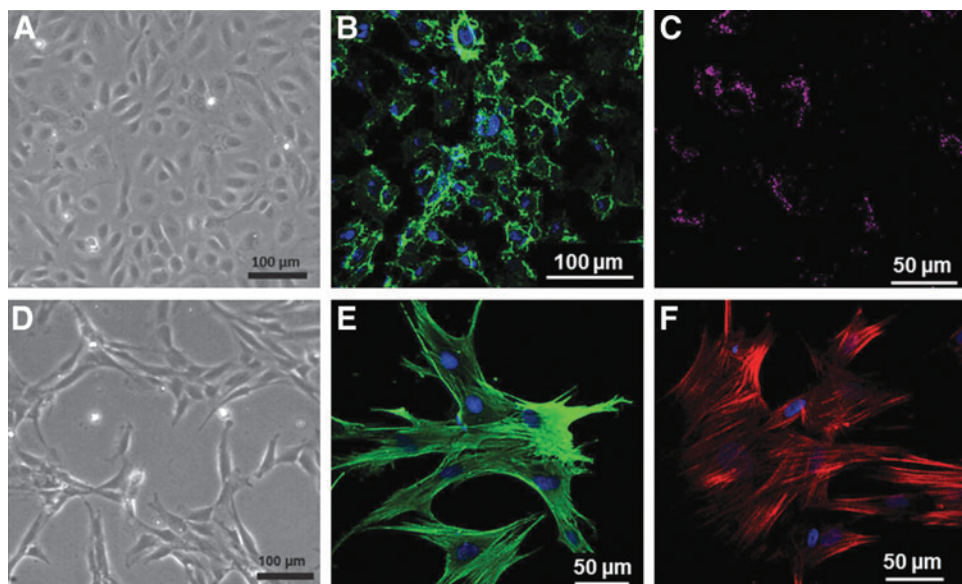

FIG. 3. Characterization of human umbilical vein endothelial cells (HUVECs) and pericytes. **(A, D)** The representative phase-contrast light microscopic images showing the characteristic morphology of HUVECs and transforming growth factor-beta (TGF-β)-induced pericyte phenotype of hMSCs. **(B)** The representative confocal microscopic image showing the immunostaining of HUVECs against CD-31 and **(C)** the image showing low-density lipoprotein uptake. **(E, F)** The confocal images of pericytes showing positive immunoreactivity against smooth muscle actin and calponin, respectively.

FIG. 4. *In vitro* vascularization in the angiogenic zones. **(A)** The representative confocal microscopic image of capillary network formation at 3 days visualized by calcein staining in the angiogenic zone. **(B, C)** The images showing the clear morphology of the vessel structure at day 5. **(D)** The magnified optical slices of **C** showing clear lumen of the vessel.
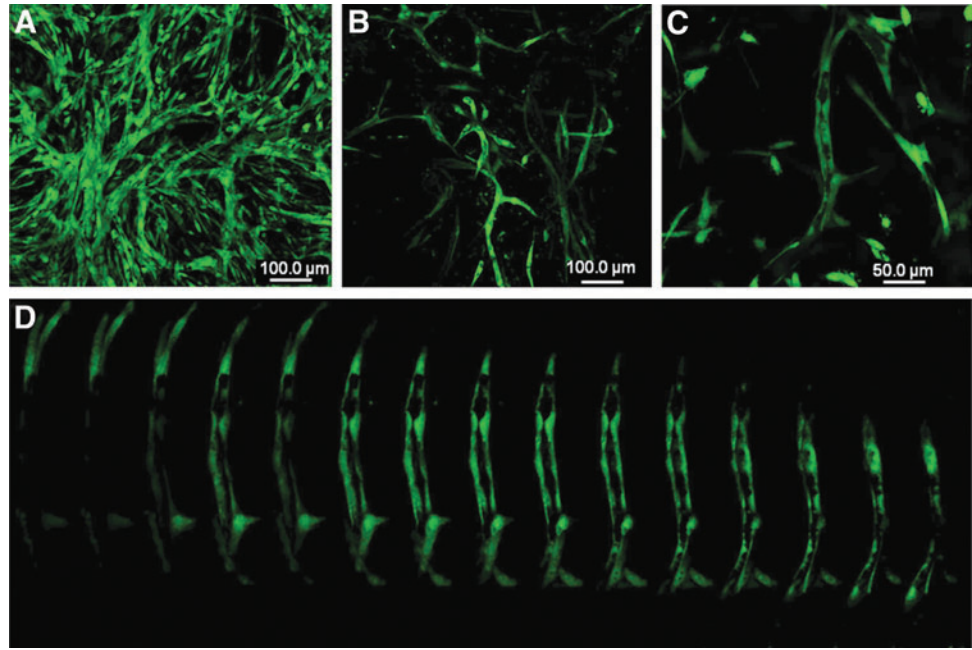
pericyte phenotype as shown in Figure 3D. They uniformly stained positive for smooth muscle cell markers such as smooth muscle actin and calponin as shown in Figures 3E and F.

Irrespective of the scaffolding platform, HUVECs and pericytes developed as microvessel-like networks *in vitro* in collagen/fibronectin gel as shown in Figure 4. At day 3, it appeared as a complex network without a clear lumen (Fig. 4A), which transformed as well-organized tubes with a lumen (Figs. 4B–D) by day 5 in endothelial growth media. Vascular network formed by prelabeled HUVECs and

pericytes showed that the vessel structure is formed by endothelial cells and the pericytes remained as supportive cells (Fig. 5) as previously reported.[34]

Multilayered constructs. The SEM images through the cross section of the multilayered constructs showed a hierarchical organization of micro- and nanoscale structural features and pores. The total thickness of the construct was dependent on the number of structural units (development and characterization of macroscopic three-dimensional layered constructs section) used for developing the construct.

FIG. 5. Compartmentalization of HUVECs and pericytes as vascular networks and supporting cells *in vitro*. **(A, B)** The respective confocal images showing the *red* dye-labeled HUVECs and the *green* dye-labeled pericytes. **(C)** The representative confocal image of organization of endothelial cells as capillary-like networks in the angiogenic zone at 3 days and **(D)** the high-magnification image clearly showing the organization of HUVECs and pericytes.
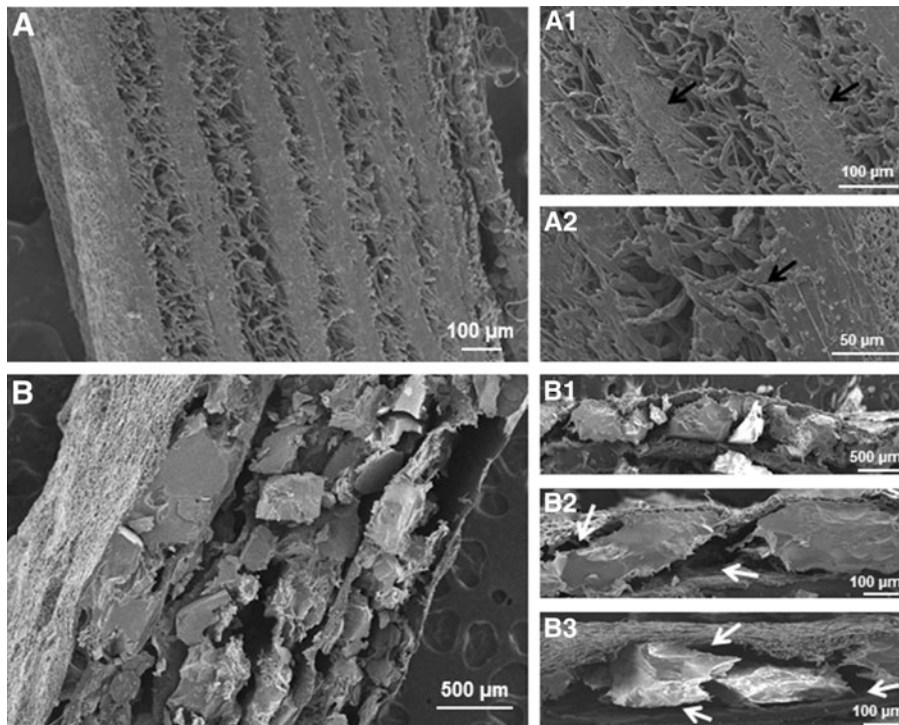
● HUVECs   ● Pericytes
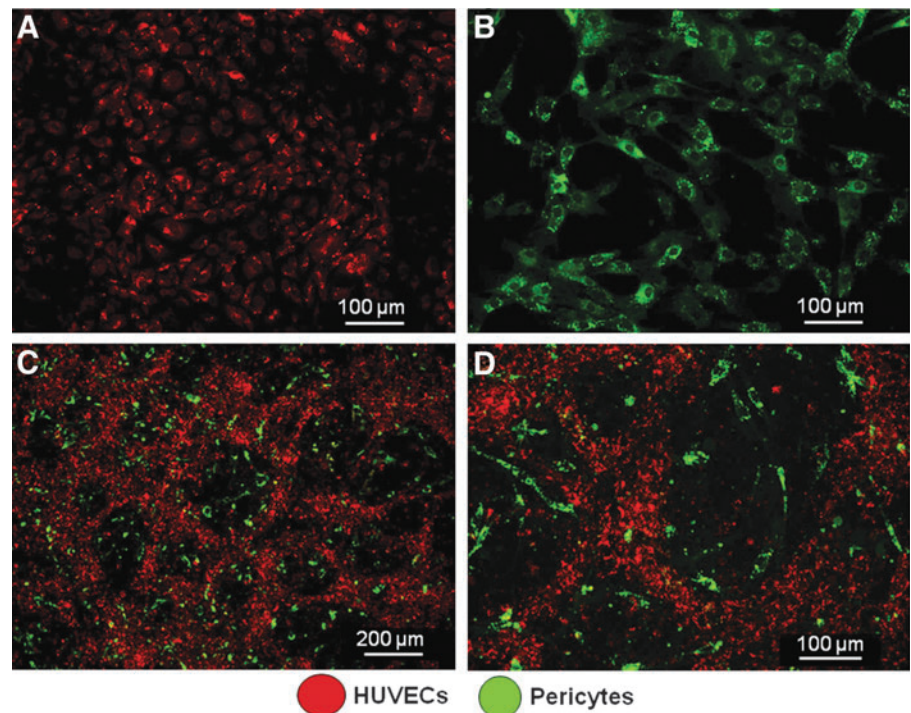
FIG. 6. Representative SEM images of the two different types of osteogenic–osteoconductive layered constructs. **(A)** Represents the layered constructs in which microfiber is used as the osteoconductive layer. **(B)** Represents the layered constructs in which ceramic is used the osteoconductive layer. **(A1, A2)** The higher magnification images of **A**, showing the limited pore size at the osteogenic–osteoconductive interface (*black arrows*). **(B1–B3)** The higher magnification images of **B**, showing the large pores in the osteogenic–osteoconductive interface (*white arrows*).

Compared with nanofiber–microfiber constructs (Figs. 6A, A1, A2), nanofibrous ceramic construct showed large pores, which have continuous channels that might have extended through the thickness of the construct (Figs. 6B, B1–B3) at the interface of osteogenic–osteoconductive zones. Moreover, it had significantly large compressive strength compared with nanofiber–microfiber constructs (Fig. 7).

Through-the-thickness vascularization in the constructs in vivo. At 4 weeks *in vivo*, the constructs maintained integrity and were enveloped by a thin fibrous capsule with minimal inflammatory reaction and remained attached to the skin as shown in Figure 8B. No delamination was visually detected from the layered constructs at the time of harvest. However, interconnected layers were visible in histological sections (Figs. 8C, D).
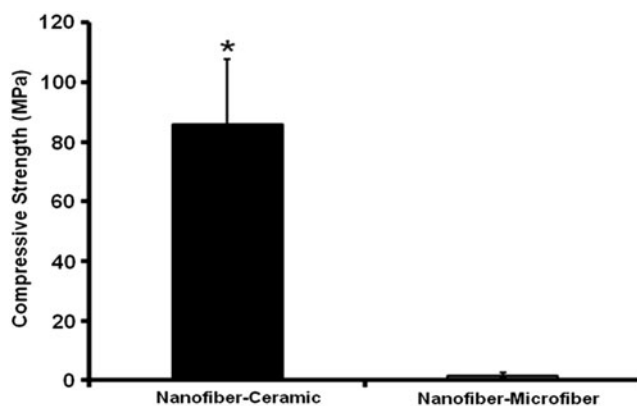
The gross appearance of vascularization around the implanted constructs was more or less similar in all the constructs. Figures 8A and B show the representative photographs showing the vascularization around the implanted engineered construct. Much more well-defined and clear vascularization was evident in the constructs containing the ceramic osteoconductive layers in the presence of angiogenic zone at the interface (Figs. 10A, B, D, E). When microfibrous osteoconductive layers were used in the presence of angiogenic zone at the interface, vascularization does occur, but not as effectively (Figs. 9A, B, D, E). Interestingly, the absence of angiogenic cells in the angiogenic zone had no effect on the vascularization of the construct in the nanofiber–ceramic construct (Figs. 10D, E). This was not the case in the nanofiber/microfiber constructs wherein the presence of cells in the angiogenic zone was critical (Figs. 9D, E). Constructs without the angiogenic zone at the interface of layers had no vascularization on both nanofiber–ceramic as well as nanofiber–microfiber constructs (Figs. 9C, F and 10C, F).

The semiquantitative evaluation of the vessel density revealed that the nanofiber–ceramic constructs with the angiogenic zone ($N^{C+}C^{G+C+}$ and $N^{C+}C^{G+C-}$) at the interface had significantly large number of functional vessels (40–50 μm diameter) inside the construct compared with nanofiber–microfiber constructs with the angiogenic zone ($N^{C+}M^{G+C+}$ and $N^{C+}M^{G+C-}$) at the interface (Fig. 11). There were no statistically significant differences in the number or size of vessels present in nanofiber–ceramic constructs with the angiogenic zone with or without cells. Interestingly, we were not able to observe vessels inside the constructs without the angiogenic zone at the interface of the layers in nanofiber–microfiber layered constructs. We have also analyzed the density of vessels in the core area (middle of two structural units sliced at the center) of the construct (Fig. 12).

FIG. 7. Compressive strength of nanofiber–ceramic and nanofiber–microfiber constructs. (*$p<0.05$).

FIG. 8. Hematoxylin and eosin-stained histological images showing vascularization and integration of the construct with the host tissue. **(A)** Represents the host vessel coverage on the construct within a week after implantation and **(B)** shows the integration of the construct with the subcutaneous tissue of the skin. **(C, D)** Represent histological images showing the layered architecture of nanofibrous ceramic and nanofibrous–microfibrous constructs, respectively, at 4 weeks *in vivo*.
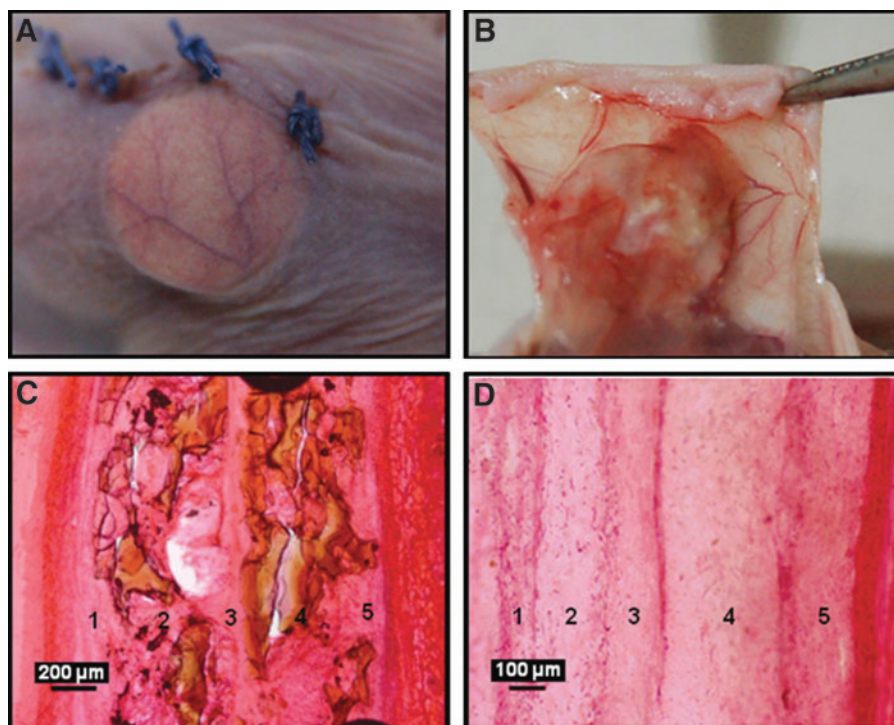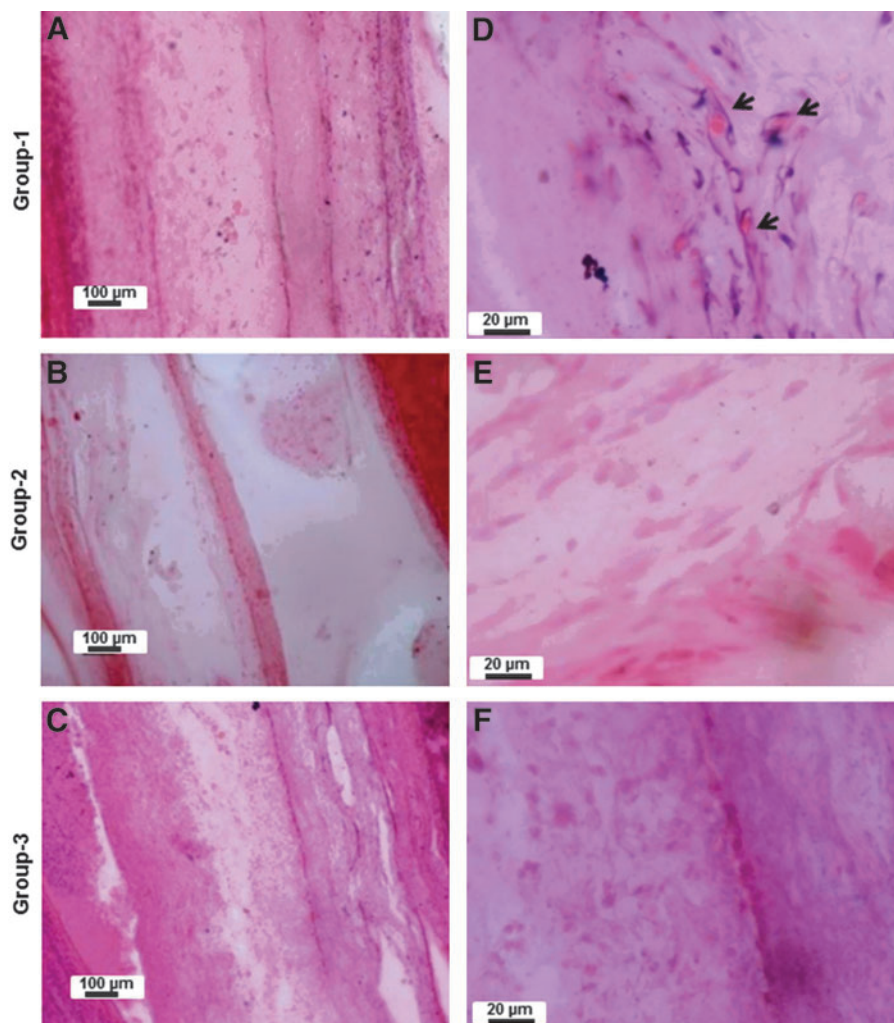

FIG. 9. Hematoxylin and eosin-stained histological images showing the vascularization inside the nanofibrous–microfibrous layered constructs. **(A–C)** The representative low-magnification representative images of the layered constructs with angiogenic zone containing cells (group-1: $N^{C+}M^{G+C+}$), angiogenic zone without cells (group-2: $N^{C+}M^{G+C-}$), and without angiogenic zone (group-3:$N^{C-}M^{G-C-}$), respectively (Table 1). Respective higher magnification images are shown **(D–F)**. The *arrowheads* show the vessels in the constructs.

FIG. 10. Hematoxylin and eosin-stained histological images showing the vascularization inside the nanofibrous ceramic layered constructs. **(A–C)** The representative low-magnification images of the layered constructs with the angiogenic zone containing cells (group-1: $N^{C+}C^{G+C+}$), angiogenic zone without cells (group-2: $N^{C+}C^{G+C-}$), and without angiogenic zone (group-3: $N^{C-}C^{G-C-}$), respectively (Table 1). Respective higher magnification images are shown **(D–F)**. The *arrowheads* show the vessels in the constructs.
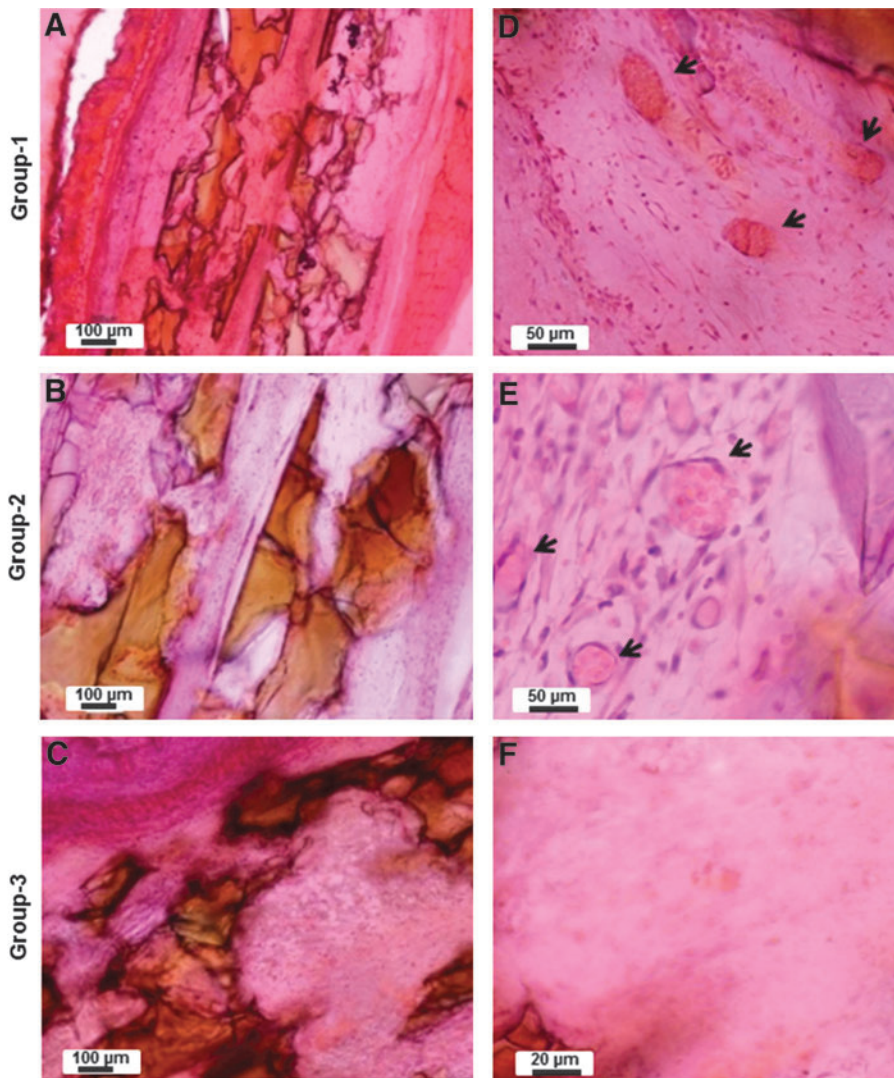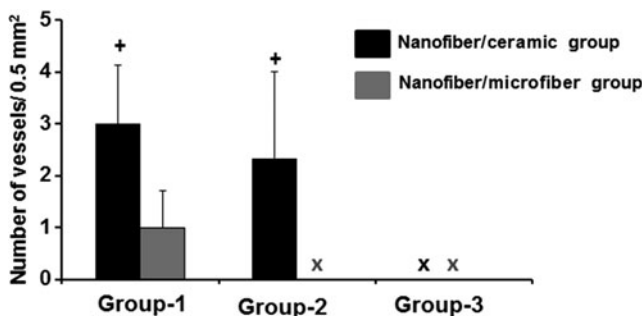

FIG. 11. Semiquantitative analysis of the vascularization of the constructs. Graph represents the number of vessels identified with diameters in the range of 40–50 μm. The error bars represent average ± standard deviation of four fields of $0.5 \times 0.5 \, mm^2$ from four different sections ($^+p < 0.05$). The number of capillaries in nanofiber–ceramic constructs ($N^{C+}C^{G+C+}$) and ($N^{C+}C^{G+C-}$) compared with nanofiber–microfiber constructs in group-1 ($N^{C+}M^{G+C+}$) and group-2 ($N^{C+}M^{G+C-}$).

The trend in vascularization in the core was also the same as seen above (Fig. 12A–E). Nanofiber–microfiber constructs showed significantly lower number of vessels compared with nanofiber–ceramic groups, and the presence of cells in the angiogenic zone had no effect on vascularization in nanofiber–ceramic constructs.

No sign of mature bone formation was observed in the constructs at 4-week time in the ectopic site. However, EDS analysis showed mineralization (C/P > 1.67) in the MSC-seeded nanofibers from the constructs at 4 weeks *in vivo*. The spectra from nanofibers without MSCs showed relatively low counts of the minerals and showed a calcium/phosphate ratio less than 1.67. Figure 13 shows the representative spectra showing the Ca/P ratio in the constructs.

Discussion

This study was aimed to investigate the possibility of achieving through-the-thickness vascularization in the engineered layered construct by spatially separating the individual layers by few hundred microns with intercalating angiogenic zones. The influence of endothelial cells and supporting cells in the angiogenic zone to attain vascularization of
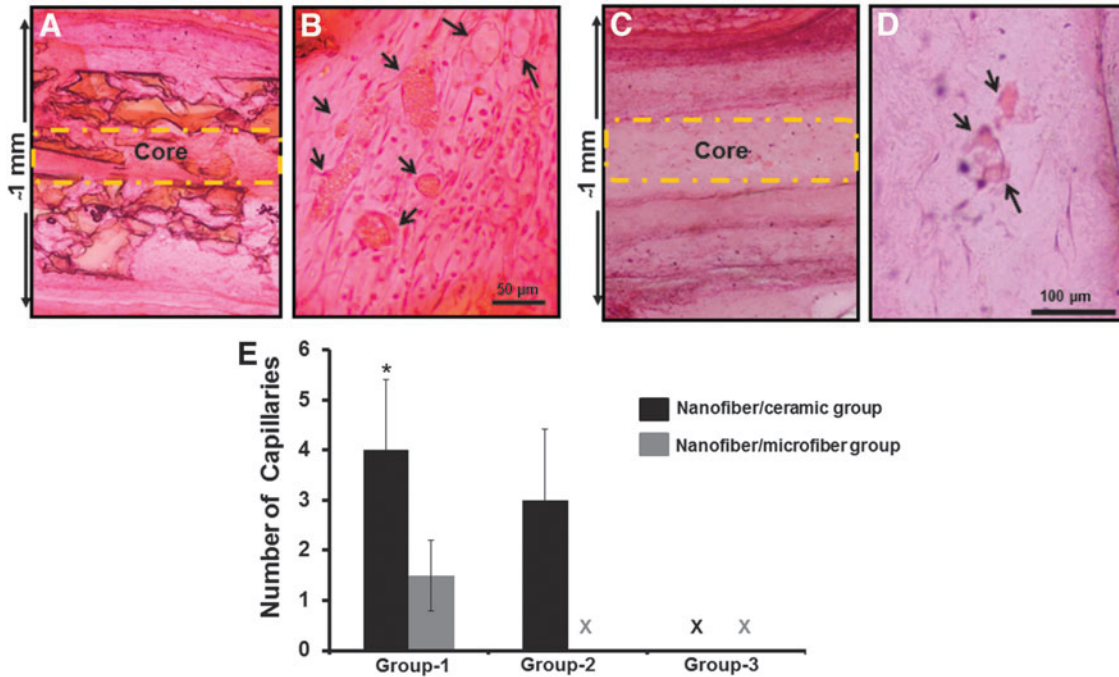
FIG. 12. Through-the-thickness vascularization of the layered constructs. **(A, C)** The representative hematoxylin and eosin-stained low-magnification histological images showing all the layers of nanofibrous–microfibrous as well as nanofibrous ceramic constructs, respectively. **(B, D)** The representative images showing the presence of functional vessels (*arrows*) at the interface in *middle* of the construct. **(E)** The semiquantification of the number of capillaries present in the core of the construct. $*p < 0.05$ compared with the number of capillaries in nanofibrous ceramic ($N^{C+}C^{G+C+}$) and nanofibrous–microfibrous ($N^{C+}M^{G+C+}$) constructs.
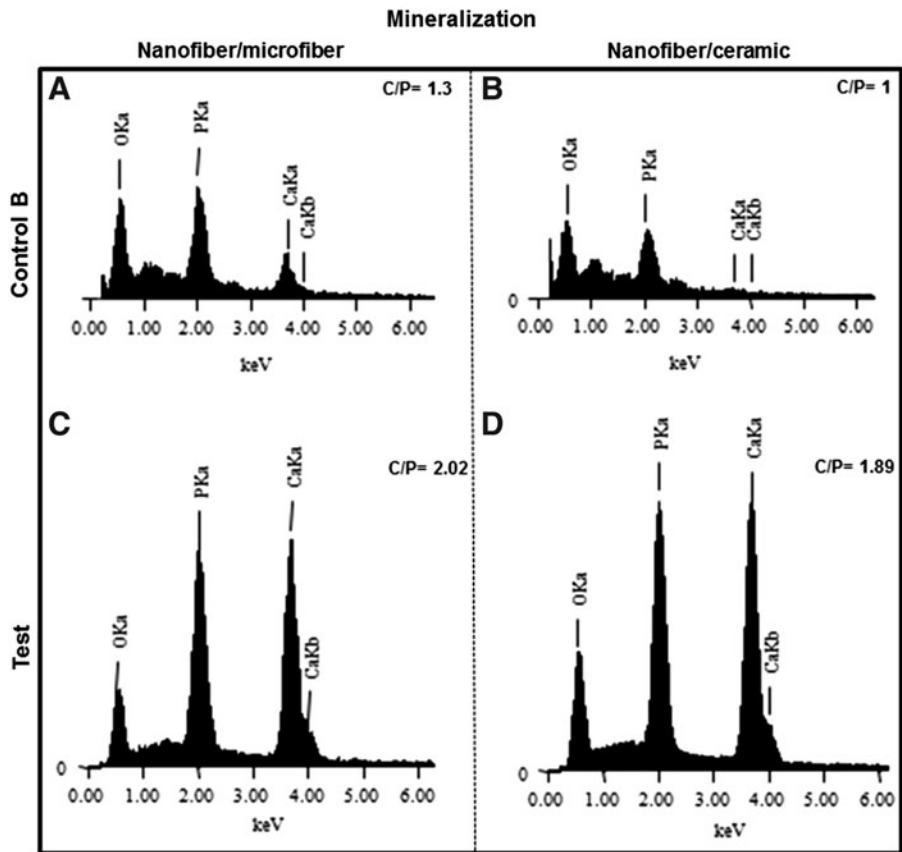
FIG. 13. Calcium/phosphate ratio in the nanofibers of the implanted constructs. Energy-dispersive X-ray spectroscopy (EDS) spectra of nanofibers extracted from nanofiber–microfiber **(A)** and nanofiber–ceramic **(B)** constructs at 4 weeks of *in vivo* implantation, which were not seeded with MSCs ($N^{C-}M^{G-C-}$ and $N^{C-}C^{G-C-}$). **(C, D)** The EDS spectra of respective constructs, which were seeded with MSCs ($N^{C+}M^{G+C-}$ and $N^{C+}C^{G+C-}$), at 4 weeks of *in vivo* implantation.

FIG. 14. Pictorial representation of the layered constructs and the proposed pattern of through-the-thickness vascularization.

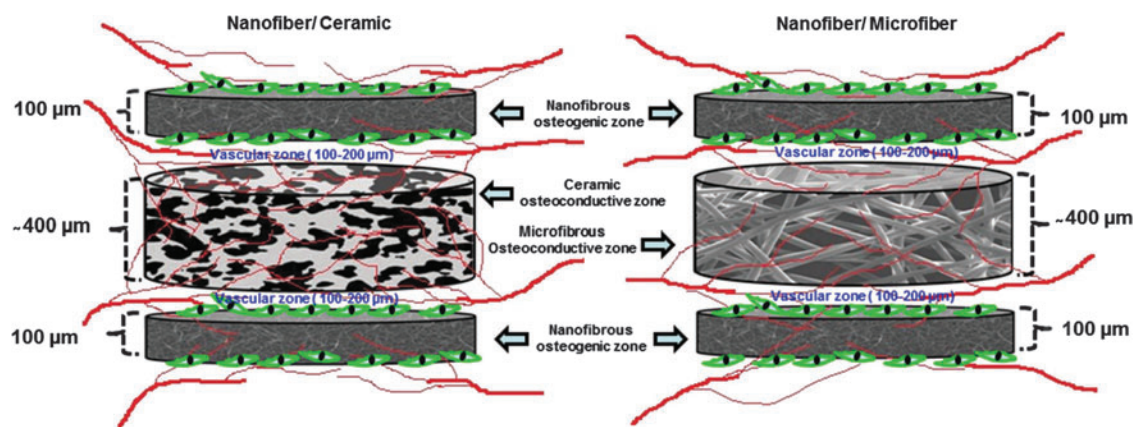the layered construct was also investigated. Pham *et al.*[21] have previously investigated the potential of multilayered scaffolds made of alternating layers of nanofibers and microfibers for 3D tissue engineering applications. They reported the role of fiber size and thickness of the layers on cell infiltration and cell spreading. However, the potential of the multilayered scaffolds in vascularizing the construct through the interface of the layers and its effect on bone formation have not been investigated before. The possibility of achieving through-the-thickness vascularization without using cells in the angiogenic zone was of particular interest due to its potential as a more off-the-shelf approach. We hypothesized that vessels from the host would be able to grow through the thickness of the construct by providing a layered architecture with continuous channels at the interface of the layers with a favorable microenvironment as shown in Figure 14. We separately engineered porous osteoconductive layers and nanofibrous osteogenic layers in microscale thickness and incorporated a favorable microenvironment for vascularization between the layers. This particular design was expected to guide host vessels, which reach the periphery of the layered construct, into the core of the construct through the interface of the layers. By providing a favorable environment for vessel ingrowth through the interface of layers within every 500 μm (Fig. 6), this design ensured the presence of vessels within the diffusion limit of oxygen (100–200 μm) from any cells/tissue growing in the construct. In addition to the presence of functional vessels from the host, we expected vasculogenesis as observed *in vitro* in the angiogenic zone (Fig. 4) in groups with endothelial and supporting cells.

Several investigators have investigated the importance of pore size in vascularization on various scaffolding platforms. Capillary ingrowth from the surrounding tissue and vascularization of the scaffolds by migration of endothelial cells are affected by the pore-related parameters of the scaffolds.[16,38] Pore size in the range of 100–400 μm has generally been accepted to be favorable for functional vascularization compared with smaller pore sizes.[19,38,39] The nanofiber–ceramic layered constructs developed and used in this study had pore sizes in the range of 100–400 μm at the interface (Figs. 6B1–B3) compared with the nanofiber–microfiber constructs, which had pores smaller than 100 μm

at the interface of the layers. This near-interface porous region is expected to contain the collagen/fibronectin gel, thereby potentially favoring vascular ingrowth at the interface. The significant increase in vascularization observed in the nanofiber–ceramic constructs can be attributed to the relatively large pore sizes in the nanofiber–ceramic constructs. The apparent lack of need for cells in the angiogenic zone in these constructs suggests the potential of layered constructs in overcoming one of the crucial challenges in tissue engineering, namely that of access to the interior of the constructs of vasculature outside of the construct. The presence of the angiogenic gel layer was crucial for developing overall through the thickness vascularization of the construct. We found that nanofiber–ceramic layered constructs without the angiogenic zone failed to facilitate functional vascularization in the layered constructs. Thus, it appears that vascularization of the osteogenic zones can only occur efficiently once the vascular access is provided to the bulk of the construct through the gel layers within the pores at the interface between the osteogenic and osteoconductive layers. The osteoconductive layers also need a favorable environment for further access of vasculature into the osteoconductive region. This results from endothelial migration, which is essential to angiogenesis.[40] Such secondary access is usually not favored beyond about 400 μm thickness, hence the present construct bioengineered to provide such primary access to the vasculature along the interface can possibly be a critical step in the success of this construct.

We have provided the vasculogenic/angiogenic microenvironment at the interfaces of the construct using fibronectin-containing collagen. Fibronectin-containing collagen gel has been previously reported to be favorable for vascularization.[33,36] They demonstrated that MSCs and endothelial cells on fibronectin-containing collagen gel in porous PLGA scaffolds develop vessels, which achieve anastomosis with host vasculature *in vivo*. However, they found that the presence of MSCs and endothelial cells is essential for developing functional vessels. We hypothesized that the collagen fibronectin microenvironment in the interfaces between the layers would act as angiogenic zones even under acellular conditions. Gelation of the angiogenic zone was carried out between the osteogenic–osteoconductive layers and it allowed

penetration of the gel-forming solution into the pores as well. What we observed was that the vessels developed at the interface of the nanofibrous osteogenic layer and ceramic osteoconductive layer and then further infiltrated into the macropores of the osteoconductive layers. However, the small vessels observed in the nanofibrous–microfibrous interface tend to remain at the interface (Supplementary Fig. 4) without secondary penetration into the layers, which also suggests the need for relatively large pores and the need for developing individual layers at microscale thickness (>400 micrometer) for efficient mass transport. The results indicated that growth of vessels through the vessel-permeable zone (angiogenic zone) and the presence of functional vessels in the angiogenic zone can be favorably exploited to facilitate angiogenesis and satisfy the mass transport requirement in the nearby areas by introducing a layered design as shown above (Fig. 14).

Mechanical properties of the construct also play a crucial role in bone tissue engineering.[41] Even though the engineered tissue cannot initially match the mechanical properties of the anatomical site into which it is to be implanted, it must be stable enough to allow surgical handling during implantation.[42] The layered nanofiber–ceramic construct developed in this study had a compressive strength of ~100 MPa, which is much higher than human cancellous bone, but lower than cortical bone.[43] The increase in compressive strength in the nanofiber–ceramic constructs could be attributed to the compressive strength of porous HAp, which is reported to be around 60 MPa.[43] It has been previously shown that incorporation of micro- and nanofibers with scaffolds improves the scaffold strength and stiffness.[44,45] Similar to their finding, the presence of polymeric nanofibers between the ceramic layers improved the mechanical properties of the ceramic layers (strength close to 90 MPa, as opposed to the reported value of 60 MPa, see Fig. 7), which would be advantageous to bone tissue engineering.

MSCs induced for osteogenic differentiation for 4 days were seeded on the nanofibrous discs and were used in the constructs as exogenic source of osteogenic cells. Preculture period of 4 days has been identified as optimal for bone formation *in vivo*.[46] The role of fiber diameter on porosity and cell infiltration has also been reported previously.[24] Even though the nanofibers used as osteogenic layers were <100 μm in thickness, cells remained as a single layer above the wafer. However, microfibers had enough porosity for cell infiltration across the thickness (Supplementary Fig. 5). Therefore, dual seeding (seeding on both sides of the wafer) (Fig. 2A) was performed to incorporate maximum number of cells and to ensure cell interaction across the layers. On the other hand, microfibers facilitated cell infiltration across the thickness.

Endothelial cells in combination with TGF-β-treated MSCs developed pericyte markers and formed vessel-like structures *in vitro* in the collagen/fibronectin gel (Fig. 4). The capillary-like tubes developed in the gel with clear lumen indicated the angiogenic/vasculogenic environment of the gel. Even though it developed as distinct capillaries *in vitro*, implanting it *in vivo* was challenging mainly due to the unfavorable environment soon after the surgical procedure. To get an understanding of the survival rate of the implanted cell viability, we have separately implanted nanofibrous discs seeded with MSCs in to the flanks and found

that cell death was around 50% and the cells, which were spread *in vitro*, became round cells after 48 h *in vivo* (Supplementary Fig. 6). This would possibly be an indication of the unfavorable immediate environment, which cells may have to face soon after implantation. However, further studies are necessary for understanding the reason behind the morphology change, which we observed *in vivo*.

The implanted constructs were harvested at 4 weeks from the implantation site and longitudinal sections were made through the middle of the constructs, and HE staining was performed to evaluate the through-the-thickness vascularization. Vessels with an internal diameter of 40–50 μm were considered as large and functional vessels capable for perfusion. We were able to observe a good number of functional vessels (with red blood cells inside) within the layers of scaffolds, indicating that the design philosophy of the layered scaffolding system facilitated through-the-thickness vascularization. There were two interesting observations. First, the number and size of vessels observed in the nanofiber–microfiber constructs were significantly lower compared with nanofiber–ceramic constructs regardless of the presence or absence of cells in the angiogenic zone. It suggests the requirement of continuous channels, which run through the entire length of the constructs at the interface of the layers. As shown in Figure 6A, nanofiber–microfiber constructs had relatively smaller pores compared with the ceramic construct and this may have played a role in controlling the secondary access of the vasculature. Second, there was no statistically significant difference in the number for functional vessels in the angiogenic zone with or without cells. This suggests that collagen/fibronectin gel alone is enough for developing functional vessels in the layered design and it is not critical to introduce endothelial/pericyte cells into this layer. This would be of great importance in the translational aspect.

Even though very good through-the-thickness vascularization was observed in the osteogenic–osteoconductive ceramic groups, we could not observe significant bone formation at the 4-week time point in any of the groups. Previous studies also reported no bone formation in MSC-seeded porous ceramics at 4 weeks[47,48] and might suggest evaluation at longer time period for bone formation. However, there was mineralization on the nanofibers, which were seeded with MSCs on both groups, which would suggest that the calcium/phosphate ratio observed in the MSC-seeded constructs was due to the mineralized ECM produced by seeded MSCs.

Another reason for the lack of bone formation may be the animal model itself. This is a subcutaneous model rather than a bone defect model, hence recruitment of MSCs and osteoblasts cannot be expected, similar to orthotopic sites for bone. At ectopic sites, bone formation directly depends on the incorporated bone-forming cells. The less than optimal conditions of incorporated MSCs immediately after surgery (Supplementary Fig. 6) could delay bone formation in cell-seeded constructs.

Conclusion

The potential of achieving through-the-thickness vascularization in tissue-engineered constructs has been successfully demonstrated using layered design with microscale

thick individual layers. Our results indicated that thickness of the layers, size of the pores, and the vascular environment at the interface of the layers are crucial factors to attain through-the-thickness functional vascularization in the engineered construct. The best construct appears to be one wherein there is an angiogenic layer at the interface between an osteogenic and an osteoconductive layer. This angiogenic layer, even in the absence of exogenous endothelial cells and pericytes, provided internal primary access of the external vasculature into the construct. Once the primary access is achieved, the vasculature is able to gain secondary access to the osteoconductive layers because of their microporous nature and because of its small thickness (400 μm thickness). In the absence of the angiogenic gel-based layer, vascularization was found to be absent in the macroscopic construct.

Acknowledgments

Disclosure Statement

No competing financial interests exist.

References

1. Jain, R.K., Au, P., Tam, J., Duda, D.G., and Fukumura, D. Engineering vascularized tissue. Nat Biotechnol **23,** 821, 2005.
2. Kaully, T., Kaufman-Francis, K., Lesman, A., and Levenberg, S. Vascularization—the conduit to viable engineered tissues. Tissue Eng Part B Rev **15,** 159, 2009.
3. Bramfeldt, H., Sabra, G., Centis, V., and Vermette, P. Scaffold vascularization: a challenge for three-dimensional tissue engineering. Curr Med Chem **17,** 3944, 2010.
4. Santos, M.I., and Reis, R.L. Vascularization in bone tissue engineering: physiology, current strategies, major hurdles and future challenges. Macromol Biosci **10,** 12, 2010.
5. Lovett, M., Lee, K., Edwards, A., and Kaplan, D.L. Vascularization strategies for tissue engineering. Tissue Eng Part B Rev **15,** 353, 2009.
6. Kang, Y., Mochizuki, N., Khademhosseini, A., Fukuda, J., and Yang, Y. Engineering a vascularized collagen-beta-tricalcium phosphate graft using an electrochemical approach. Acta Biomater **11,** 449, 2015.
7. Kang, Y., Ren, L., and Yang, Y. Engineering vascularized bone grafts by integrating a biomimetic periosteum and beta-TCP scaffold. ACS Appl Mater Interfaces **6,** 9622, 2014.
8. Amini, A.R., and Nukavarapu, S.P. Oxygen-tension controlled matrices for enhanced osteogenic cell survival and performance. Ann Biomed Eng **42,** 1261, 2014.
9. Druecke, D., Langer, S., Lamme, E., Pieper, J., Ugarkovic, M., Steinau, H.U., and Homann, H.H. Neovascularization of poly(ether ester) block-copolymer scaffolds in vivo: long-term investigations using intravital fluorescent microscopy. J Biomed Mater Res A **68,** 10, 2004.
10. Gerecht, S., Townsend, S.A., Pressler, H., Zhu, H., Nijst, C.L., Bruggeman, J.P., Nichol, J.W., and Langer, R. A porous photocurable elastomer for cell encapsulation and culture. Biomaterials **28,** 4826, 2007.
11. Landers, R., Hubner, U., Schmelzeisen, R., and Mulhaupt, R. Rapid prototyping of scaffolds derived from thermoreversible hydrogels and tailored for applications in tissue engineering. Biomaterials **23,** 4437, 2002.
12. Mehdizadeh, H., Sumo, S., Bayrak, E.S., Brey, E.M., and Cinar, A. Three-dimensional modeling of angiogenesis in porous biomaterial scaffolds. Biomaterials **34,** 2875, 2013.
13. Novosel, E.C., Kleinhans, C., and Kluger, P.J. Vascularization is the key challenge in tissue engineering. Adv Drug Deliv Rev **63,** 300, 2011.
14. Moon, J.J., and West, J.L. Vascularization of engineered tissues: approaches to promote angio-genesis in biomaterials. Curr Top Med Chem **8,** 300, 2008.
15. Johnson, P.C., Mikos, A.G., Fisher, J.P., and Jansen, J.A. Strategic directions in tissue engineering. Tissue Eng **13,** 2827, 2007.
16. Patel, Z.S., and Mikos, A.G. Angiogenesis with biomaterial-based drug- and cell-delivery systems. J Biomater Sci Polym Ed **15,** 701, 2004.
17. Laschke, M.W., and Menger, M.D. Vascularization in tissue engineering: angiogenesis versus inosculation. Eur Surg Res **48,** 85, 2012.
18. Rouwkema, J., Rivron, N.C., and van Blitterswijk, C.A. Vascularization in tissue engineering. Trends Biotechnol **26,** 434, 2008.
19. Feng, B., Jinkang, Z., Zhen, W., Jianxi, L., Jiang, C., Jian, L., Guolin, M., and Xin, D. The effect of pore size on tissue ingrowth and neovascularization in porous bioceramics of controlled architecture in vivo. Biomed Mater **6,** 015007, 2011.
20. Bai, F., Wang, Z., Lu, J., Liu, J., Chen, G., Lv, R., Wang, J., Lin, K., Zhang, J., and Huang, X. The correlation between the internal structure and vascularization of controllable porous bioceramic materials in vivo: a quantitative study. Tissue Eng Part A **16,** 3791, 2010.
21. Pham, Q.P., Sharma, U., and Mikos, A.G. Electrospinning of polymeric nanofibers for tissue engineering applications: a review. Tissue Eng **12,** 1197, 2006.
22. Samavedi, S., Whittington, A.R., and Goldstein, A.S. Calcium phosphate ceramics in bone tissue engineering: a review of properties and their influence on cell behavior. Acta Biomater **9,** 8037, 2013.
23. Ma, Z., Kotaki, M., Inai, R., and Ramakrishna, S. Potential of nanofiber matrix as tissue-engineering scaffolds. Tissue Eng **11,** 101, 2005.
24. Pham, Q.P., Sharma, U., and Mikos, A.G. Electrospun poly(epsilon-caprolactone) microfiber and multilayer nanofiber/microfiber scaffolds: characterization of scaffolds and measurement of cellular infiltration. Biomacromolecules **7,** 2796, 2006.
25. Zhong, S., Zhang, Y., and Lim, C.T. Fabrication of large pores in electrospun nanofibrous scaffolds for cellular infiltration: a review. Tissue Eng Part B Rev **18,** 77, 2012.
26. Guimaraes, A., Martins, A., Pinho, E.D., Faria, S., Reis, R.L., and Neves, N.M. Solving cell infiltration limitations

of electrospun nanofiber meshes for tissue engineering applications. Nanomedicine **5,** 539, 2010.

27. Sathy, B.N., Watson, B.M., Kinard, L.A., Spicer, P.P., Dahlin, R.L., Mikos, A.G., and Nair, S. Bone tissue engineering with multilayered scaffolds-Part II: combining vascularization with bone formation in critical-sized bone defect. Tissue Eng Part A **21,** 2495, 2015.

28. Boyde, A., Corsi, A., Quarto, R., Cancedda, R., and Bianco, P. Osteoconduction in large macroporous hydroxyapatite ceramic implants: evidence for a complementary integration and disintegration mechanism. Bone **24,** 579, 1999.

29. Cipitria, A., Skelton, A., Dargaville, T.R., Dalton, P.D., and Hutmacher, D.W. Design, fabrication and characterization of PCL electrospun scaffolds-a review. J Mater Chem **21,** 9419, 2011.

30. Binulal, N.S., Natarajan, A., Menon, D., Bhaskaran, V.K., Mony, U., and Nair, S.V. Gelatin nanoparticles loaded poly(epsilon-caprolactone) nanofibrous semi-synthetic scaffolds for bone tissue engineering. Biomed Mater **7,** 065001, 2012.

31. Shalumon, K.T., Binulal, N.S., Deepthy, M., Jayakumar, R., Manzoor, K., and Nair, S.V. Preparation, characterization and cell attachment studies of electrospun multi-scale poly(caprolactone) fibrous scaffolds for tissue engineering. J Macromol Sci A **48,** 21, 2011.

32. Binulal, N.S., Deepthy, M., Selvamurugan, N., Shalumon, K.T., Suja, S., Mony, U., Jayakumar, R., and Nair, S.V. Role of nanofibrous poly(caprolactone) scaffolds in human mesenchymal stem cell attachment and spreading for in vitro bone tissue engineering-response to osteogenic regulators. Tissue Eng Part A **16,** 393, 2010.

33. Koike, N., Fukumura, D., Gralla, O., Au, P., Schechner, J.S., and Jain, R.K. Tissue engineering: creation of long-lasting blood vessels. Nature **428,** 138, 2004.

34. Jaffe, E.A., Nachman, R.L., Becker, C.G., and Minick, C.R. Culture of human endothelial cells derived from umbilical veins. Identification by morphologic and immunologic criteria. J Clin Invest **52,** 2745, 1973.

35. Hirschi, K.K., Rohovsky, S.A., and D'Amore, P.A. PDGF, TGF-beta, and heterotypic cell-cell interactions mediate endothelial cell-induced recruitment of 10T1/2 cells and their differentiation to a smooth muscle fate. J Cell Biol **141,** 805, 1998.

36. Tsigkou, O., Pomerantseva, I., Spencer, J.A., Redondo, P.A., Hart, A.R., O'Doherty, E., Lin, Y., Friedrich, C.C., Daheron, L., Lin, C.P., Sundback, C.A., Vacanti, J.P., and Neville, C. Engineered vascularized bone grafts. Proc Natl Acad Sci U S A **107,** 3311, 2010.

37. Maciag, T., Kadish, J., Wilkins, L., Stemerman, M.B., and Weinstein, R. Organizational behavior of human umbilical vein endothelial cells. J Cell Biol **94,** 511, 1982.

38. Choi, S.W., Zhang, Y., Macewan, M.R., and Xia, Y. Neovascularization in biodegradable inverse opal scaffolds with uniform and precisely controlled pore sizes. Adv Healthc Mater **2,** 145, 2013.

39. Chiu, Y.C., Cheng, M.H., Engel, H., Kao, S.W., Larson, J.C., Gupta, S., and Brey, E.M. The role of pore size on vascularization and tissue remodeling in PEG hydrogels. Biomaterials **32,** 6045, 2011.

40. Lamalice, L., Le Boeuf, F., and Huot, J. Endothelial cell migration during angiogenesis. Circ Res **100,** 782, 2007.

41. Yang, S., Leong, K.F., Du, Z., and Chua, C.K. The design of scaffolds for use in tissue engineering. Part I. Traditional factors. Tissue Eng **7,** 679, 2001.

42. O'Brien, F.J. Biomaterials and scaffolds for tissue engineering. Mater Today **14,** 3, 2011.

43. Moore, W.R., Graves, S.E., and Bain, G.I. Synthetic bone graft substitutes. ANZ J Surg **71,** 354, 2001.

44. Albanna, M.Z., Bou-Akl, T.H., Walters, H.L., 3rd, and Matthew, H.W. Improving the mechanical properties of chitosan-based heart valve scaffolds using chitosan fibers. J Mech Behav Biomed Mater **5,** 171, 2012.

45. Prosecka, E., Rampichova, M., Litvinec, A., Tonar, Z., Kralickova, M., Vojtova, L., Kochova, P., Plencner, M., Buzgo, M., Mickova, A., Jancar, J., and Amler, E. Collagen/hydroxyapatite scaffold enriched with polycaprolactone nanofibers, thrombocyte-rich solution and mesenchymal stem cells promotes regeneration in large bone defect in vivo. J Biomed Mater Res A **103,** 671, 2015.

46. Castano-Izquierdo, H., Alvarez-Barreto, J., van den Dolder, J., Jansen, J.A., Mikos, A.G., and Sikavitsas, V.I. Pre-culture period of mesenchymal stem cells in osteogenic media influences their in vivo bone forming potential. J Biomed Mater Res A **82,** 129, 2007.

47. Kasten, P., Vogel, J., Luginbuhl, R., Niemeyer, P., Tonak, M., Lorenz, H., Helbig, L., Weiss, S., Fellenberg, J., Leo, A., Simank, H.G., and Richter, W. Ectopic bone formation associated with mesenchymal stem cells in a resorbable calcium deficient hydroxyapatite carrier. Biomaterials **26,** 5879, 2005.

48. Wang, X.J., Huang, H., Yang, F., Xia, L.G., Zhang, W.J., Jiang, X.Q., and Zhang, F.Q. Ectopic study of tissue-engineered bone complex with enamel matrix proteins, bone marrow stromal cells in porous calcium phosphate cement scaffolds, in nude mice. Cell Prolif **44,** 274, 2011.

Address correspondence to:
Shantikumar Nair, PhD
Amrita Centre for Nanosciences & Molecular Medicine
Amrita Institute of Medical Sciences and Research Centre
Amrita Vishwa Vidyapeetham University
Kochi
India

E-mail: shantinair@aims.amrita.edu